European Journal of Medicinal Chemistry 256 (2023) 115466

Contents lists available at ScienceDirect

European Journal of Medicinal Chemistry

journal homepage: www.elsevier.com/locate/ejmech

Research paper

First iron(II) organometallic compound acting as ABCB1 inhibitor

Adhan Pilon [a], Fernando Avecilla [b], Miklós Mohai [c], Éva A. Enyedy [d], Bálint Rácz [e], Gabriella Spengler [e], M. Helena Garcia [a], Andreia Valente [a,*]

[a] Centro de Química Estrutural, Institute of Molecular Sciences and Departamento de Química e Bioquímica, Faculdade de Ciências, Universidade de Lisboa, Campo Grande, 1749-016, Lisboa, Portugal
[b] Universidade da Coruña, Grupo NanoToxGen, Centro Interdisciplinar de Química y Biología (CICA), Departamento de Química, Facultade de Ciencias, Campus de A Coruña, 15071, A Coruña, Spain
[c] Research Centre for Natural Sciences, Institute of Materials and Environmental Chemistry, Magyar tudósok körútja 2, H-1117, Budapest, Hungary
[d] MTA-SZTE Lendület Functional Metal Complexes Research Group, Department of Inorganic and Analytical Chemistry, Interdisciplinary Excellence Centre, University of Szeged, Dóm tér 7, H-6720, Szeged, Hungary
[e] Department of Medical Microbiology, Albert Szent-Györgyi Medical School, University of Szeged, Semmelweis utca 6, H-6725, Szeged, Hungary

ARTICLE INFO

Keywords:
Iron-cyclopentadienyl
ABCB1 inhibitor
Cancer multidrug resistance
Colon adenocarcinoma

ABSTRACT

Five new iron (II) complexes bearing imidazole-based (Imi-R) ligands with the general formula [Fe(η^5-C_5H_5)(CO)(PPh_3)(Imi-R)][CF_3SO_3] were synthesized and fully characterized by several spectroscopic and analytical techniques. All compounds crystallize in centrosymmetric space groups in a typical "piano stool" distribution. Given the growing importance of finding alternatives to overcome different forms of multidrug resistance, all compounds were tested against cancer cell lines with different ABCB1 efflux pump expression, namely, the doxorubicin-sensitive (Colo205) and doxorubicin-resistant (Colo320) human colon adenocarcinoma cell lines. Compound 3 bearing 1-benzylimidazole was the most active in both cell lines with IC_{50} values of 1.26 ± 0.11 and 2.21 ± 0.26 μM, respectively, being also slightly selective against the cancer cells (vs. MRC5 normal human embryonic fibroblast cell lines). This compound, together with compound 2 bearing 1*H*-1,3-benzodiazole, were found to display very potent ABCB1 inhibitory effect. Compound 3 also showed the ability to induce cell apoptosis. Iron cellular accumulation studies by ICP-MS and ICP-OES methods revealed that the compounds' cytotoxicity is not related to the extent of iron accumulation. Yet, it is worth mentioning that, from the compounds tested, 3 was the only one where iron accumulation was greater in the resistant cell line than in the sensitive one, validating the possible role of ABCB1 inhibition in its mechanism of action.

1. Introduction

Nitrogen-containing heteroaromatic-based compounds are commonly present in commercial drugs [1–3]. Among these heteroaromatics, several natural and synthetic imidazole/fused imidazole rings display a wide range of pharmacological effects, including anticancer activity [4–6]. Imidazole is a five-membered heterocycle containing three carbons and two electron-rich nitrogen atoms, capable of coordination to metal ions. In this frame, there are two iconic anticancer metal compounds that have progressed into Phase I/II clinical trials, namely NAMI-A [7,8], and KP1019, now replaced in the clinical trials by its more soluble sodium salt NKP1339/BOLD-100 [9,10], where the imidazole/fused imidazole is directly coordinated to the ruthenium (III) center. In the last years, other imidazole-based complexes, such as V(IV) [11], Os(III) [12], Au(I) [13], Cu(II) [14], Co(II) [15], Zn(II) [15], Ru(II) [16], Pd(II) [17] and Pt (II) [17–19], to name a few, have been tested in several cancer cell lines with some success. Fewer examples are found for imidazole-based iron complexes. Among them, an Fe(II)-containing salophen complex with an imidazole ligand has shown remarkable activity against six human cancer cell lines using 24 h incubation time (osteosarcoma - HOS, breast adenocarcinoma – MCF7, epithelial adenocarcinoma - A549, cervical carcinoma - HeLa, ovarian carcinoma - A2780, and malignant melanoma - G-361) [20]. Also, salen-type Fe(III) complexes [Fe(III) (salen) (L)]$_n$ where L is imidazole or benzimidazole were tested against chronic myelogenous erythroleukemia (K562) and breast adenocarcinoma (MCF7) after 72 h incubation showing good cytotoxicity [21]. Regarding iron organometallic compounds bearing coordinated imidazole-type ligands, only one example previously

* Corresponding author.
E-mail address: amvalente@ciencias.ulisboa.pt (A. Valente).

https://doi.org/10.1016/j.ejmech.2023.115466
Received 21 March 2023; Received in revised form 3 May 2023; Accepted 5 May 2023
Available online 6 May 2023

reported by some of us is found [22]. In this study, four compounds of general formula [Fe(II)(η^5-C_5H_5)(dppe)L][CF_3SO_3], where L are imidazole based ligands and dppe is ethylenebis (diphenylphosphane), were tested against ovarian A2780 (cisplatin sensitive), breast MCF7 and cervical HeLa cells showing a better cytotoxicity than cisplatin at 72 h incubation. Actually, the interest in cyclopentadienyl iron organometallic complexes (Fe(^{5}-C_5H_5); FeCp) has been growing in the last years [23–31], probably due to the large structural diversity offered by their piano-stool structure and by the nature of the π-bonded cyclopentadienyl ring that can act both as a donor and as an acceptor group, thus changing the acceptor/donor character and reactivity of other coligands [32]. F. Marchetti et al. have reported a series of diiron complexes based on the [$Fe_2Cp_2(CO)_x$] skeleton (x = 2 or 3) and containing different bridging ligands (aminocarbyne, thiocarbyne, allenyl or vinyliminium) [24,26,27]. Cytotoxicity studies showed that among them the aminocarbyne and vinyliminium complexes displayed the best biological profile, and some of them showed noticeable IC_{50} values [24,26,27]. The mode of action for the aminocarbyne complexes seems to involve several processes and/or targets [24]. Recently, the same group reported the synthesis of cationic triiron complexes obtained through the conjugation of the ferrocenyl skeleton (Fc) with a diiron biscyclopentadienyl core through a vinyliminium linkers [28]. Most of the complexes showed good cytotoxicity against several cancer cell lines with good selectivity indexes.

Our research group has been engaged with the development of mono FeCp compounds through structure-activity studies. As mentioned above, we started by disclosing a family of [Fe(η^5-C_5H_5)(dppe)(imidazole-based)][CF_3SO_3] compounds [22]. Later on we replaced the imidazole-based ligand by nitrile-based ligands and the results showed that the compounds were very efficient against human leukemia cancer cells (HL-60) and caused cell death by either apoptosis or necrosis, depending on the nitrile used [33]. We then decided to change the nature of the phosphane-based ligand from dppe to different triphenylphosphanes affording better soluble compounds in biological relevant media ([Fe(Cp)(CO)(PR_3)(L)]^n (PR_3 = triphenylphosphane, 4-(diphenylphosphino) benzoic acid or tris(4-fluorophenyl)phosphane; when L = I, n = 0; when L = 4-aminobenzonitrile, n = +1) [34]. This study was important to realize that only the cationic compounds were active against cancer cells, leading to cell death by apoptosis. Upon these results we have enlarged our collection of compounds to include several substituents at the nitrile ligand: [Fe(η^5-C_5H_5)(CO)(PPh_3)(NCR)]$^+$; NCR = benzonitrile; 4-hydroxybenzonitrile; 4-hydroxymethylbenzonitrile; 4-aminobenzonitrile; 4-bromobenzonitrile; and 4-chlorocinnamonitrile [35]. All the compounds showed remarkable cytotoxicity in MDA-MB-231 breast and SW480 colorectal cancer-derived cell lines, with some inherent selectivity. Further studies on the SW480 cell line revealed that these compounds cause cell death by apoptosis, inhibit the formation of cancer cells colonies, and affect the actin-cytoskeleton of the cells, with exception of the hydroxylated compounds, indicating that the substituent at the nitrile-based ligand is related to the compound's biological performance [35]. Within this work, we attempt to concomitantly study the effect of the imidazole-based ligand in the 'FeCp-PPh_3' core. For that, a family of 5 compounds was synthesized bearing different substituents at the imidazole-based ligand that were chosen taking into consideration previous studies [22] and to include some more lipophilic (3 and 4) or hydrophilic (5) substituents at the imidazole (1) and also a fused ring (2).

2. Results and discussion

2.1. Synthesis

The new cationic complexes with general formula [Fe(η^5-C_5H_5)(CO)(PPh_3)(Imi-R)][CF_3SO_3] were obtained by iodide abstraction from [Fe(η^5-C_5H_5)(CO)(PPh_3)(I)] using $AgCF_3SO_3$, followed by reaction in acetone at room temperature for 24 h with the corresponding imidazole-based ligand (Scheme 1, Imi-R = 1*H*-midazole (1); 1*H*-1,3-benzodiazole (2); 1-benzylimidazole (3); 1-butylimidazole (4); 1-(2-hydroxyethyl) imidazole (5)). The reaction was followed by NMR until the total amount of the precursor was consumed and only a single Cp signal was observed in the spectrum. Pure compounds were obtained in moderate yields (44–73%) after column chromatography and recrystallization by slow diffusion. The structure of the new complexes is supported by spectroscopic data (^{1}H, ^{13}C and ^{31}P NMR, FTIR and UV–Vis). Results obtained by elemental analyses and ESI-HR confirmed their purity. In addition, single crystals of all compounds were obtained and studied by X-ray crystallography.

2.2. NMR spectroscopy

NMR characterization of the five new complexes was done in acetone-d^6, and all resonances were attributed using 1D and 2D NMR experiments, namely, ^{1}H, ^{13}C{^{1}H}-apt, ^{31}P{^{1}H}, COSY, HMQC, and HMBC for unequivocal attribution of all the signals, and follow the atom numbering presented in Scheme 1. For all compounds, there is a deshielding on the 'Cp' upon coordination of the imidazoles (+0.42 to +0.57 ppm), as expected for 'FeCp' cationic complexes. The coordination of the imidazole-based ligands to the metallic center also leads to a deshielding of the H_1 protons for complexes 1 and 2, in particular for 1 (+1.14 ppm), which could be related to the formation of a hydrogen bond between these protons and the oxygen from the triflate anion (confirmed by X-ray analyses). For complexes 3–5, substituted at N1, the coordination can be confirmed by the deshielded of H_2. ^{13}C{^{1}H} NMR data show the 'Cp' ring at the usual chemical shift for cationic Fe(II) compounds (~85 ppm) and a significant deshielding when compared to the precursor (up to +44 ppm), after the coordination of the imidazole-based ligands to the metallic center. The ^{31}P{^{1}H} spectrum is characterized by the presence of a single signal around 66 ppm for all the compounds.

2.3. FT-IR spectroscopy

The analysis of the solid state FTIR spectra (KBr pellets) of all iron complexes show the presence of the characteristic bands for the cyclopentadienyl ring and the aromatic rings of the triphenylphosphane and imidazole ligands (3200–3000 cm^{-1} and 1600–1400 cm^{-1}). Additional three bands at 1250, 1161, and 1029 cm^{-1} confirm the presence of the counter-ion $CF_3SO_3^-$. The coordination of the imidazole nitrogen to the iron center can be confirmed by the characteristic stretching vibration of the amine functional group appearing at 3400–3500 cm^{-1} which intensity and number of vibrations decreased upon coordination due to a change in the symmetry group of the molecule. The replacement of the iodide in [Fe(η^5-C_5H_5)(CO)(PPh_3)(I)] by the imidazole-based ligands in compounds 1–5 lead to a strengthening of the C≡O bond (1935 vs. 1955–1962 cm^{-1}). This significant enhancement of the C≡O bond reflects a decrease of π-backdonation to the coordinated carbonyl due the cationic nature of the new compounds and/or any other additional effect as it will be discussed below.

2.4. UV–visible spectrophotometry

The optical absorption spectra of all iron-cyclopentadienyl complexes were recorded in dimethylsulfoxide (DMSO) solutions (1.0×10^{-3} to 1.0×10^{-5} M). In Fig. 1 one can observe that all the complexes exhibit four characteristic bands: a strong absorption band at higher energy (below 300 nm) corresponding to intramolecular electronic transitions (π→π*) occurring in the aromatic ligands; a shoulder around 345 nm, that was attributed to electronic transitions occurring in the organometallic fragment {FeCp}$^+$ (by analogy with the iron parental complex [Fe(η^5-C_5H_5)$(CO)_2$I]) [34]; at ~420 nm there is a charge transition (CT) band ($600 < \varepsilon < 1000$ $M^{-1}cm^{-1}$); and another band, around 540 nm, with a value of $\varepsilon < 500$ $M^{-1}cm^{-1}$, which compatible

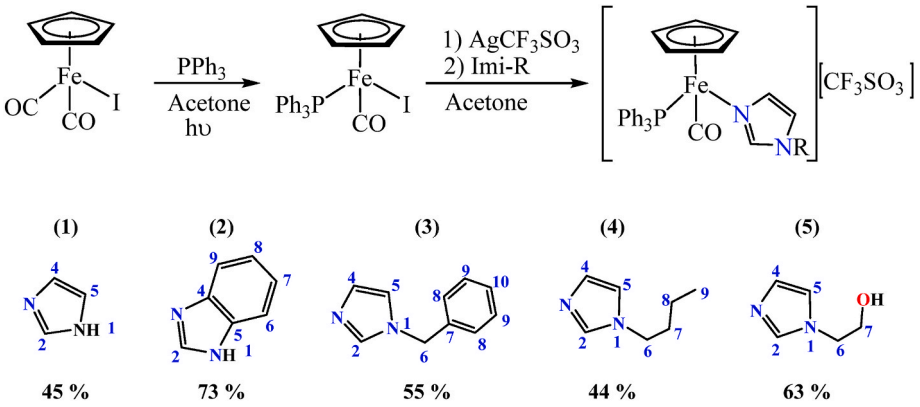

Scheme 1. Reaction scheme for the synthesis of compounds 1–5, all complexes are numbered for NMR peak assignment.

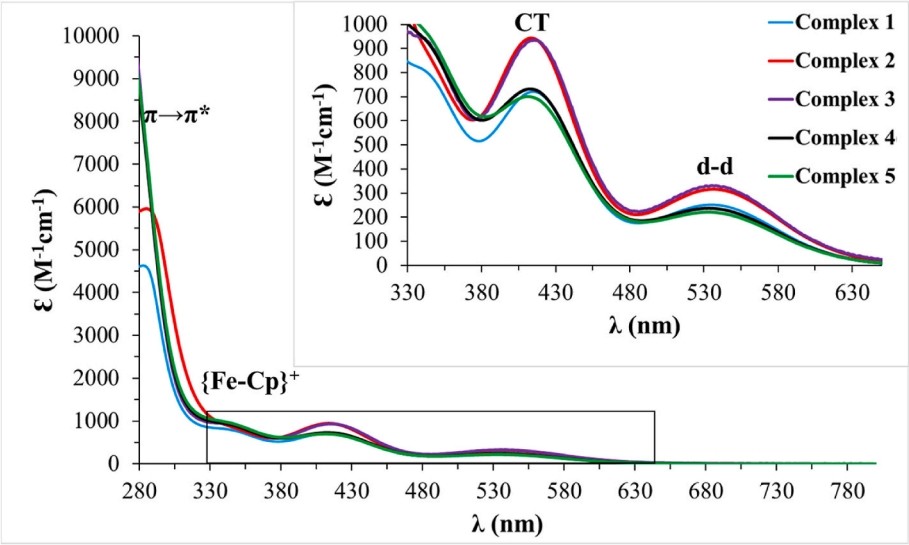

Fig. 1. Electronic spectra of complexes 1–5 in DMSO solution.

with a d-d transition band, also very common for analogous complexes [35]. The CT band seems to be a MLCT, which main contribution might be from the d_{Fe} to π* imidazole-based ligand, which is in good agreement with the overall spectroscopic data (e.g. the strengthened of the C≡O reveals a decrease of the electronic flow to the CO ligand). Nevertheless, this type of low-energy excitations involves, in general, several orbitals and it not should be excluded other contribution for this MLCT band coming from 'Fe-imidazole' to the PPh_3 coligand having in consideration our previous studies by TD-DFT calculations carried out for other FeCp related compounds [35].

2.5. Single-crystal structures of compounds 1-5

Fig. 2 depicts ORTEP representations of the cation complexes in the compounds 1–5. All the compounds crystallize in centrosymmetric space groups (see Table S1). Compound 4 has two crystallographic independent compounds in the asymmetric unit due to the disorder on butyl group. All the crystal packings contain enantiomer pairs, which we can see in Fig. S16. The iron centers adopt a "piano stool" distribution, which is formed for Fe-Cp unit, and for the PPh_3, the CO and the imidazole derived ligands. The distances between the centroid of π-cloud of cyclopentadienyl moiety to Fe center are: 1.7255 (1) Å in 1 (ring slippage, 0.041 Å), 1.7233(1) Å in 2 (ring slippage, 0.039 Å), 1.7240(6) Å in 3 (ring slippage, 0.052 Å), 1.7205(2) Å for Fe (1) and 1.7251 (2) Å for Fe (2) in 4 [ring slippage, 0.063 Å for Fe (1) and 0.050 Å for Fe (2)] and 1.7200 (1) Å in 5 (ring slippage 0.040 Å). The mean distance of metal center Fe (1) to carbon atoms of the Cp units are: 2.106 (3) Å in 1, 2.1017 (17) Å in 2, 2.097 (5) Å in 3, 2.101 (5) Å in 4 and 2.097 (2) Å in 5. The *C*–O bond lengths, 1.141 (3) Å in 1, 1.153 (2) Å in 2, 1.143 (5) Å in 3, 1.147 (7) Å in 4 and 1.151 (2) Å in 5, have a usual value for this type of compounds (see Table S2) [36].

No weak interactions between π-π clouds were observed in the crystal packing, but some short contacts and hydrogen bonds influence in the arrangement of the structures (see Table S3). Compounds 1 and 2 present interactions by hydrogen bonds between the protonate nitrogen atoms of the imidazole group and oxygen atoms of the $(CF_3SO_3)^-$ anions. In compound 1 an interaction by hydrogen bond between N (2) and O (3) was determined, with a distance donor acceptor of 3.0620 (2) Å and an angle of the 164.7°. In compound 2, due to the disorder presents on O (4), the interaction by hydrogen bond has two values, N (2)···O (4 A), with a distance between donor acceptor atoms of 2.7920 (2) Å, angle of 157.6°, and N (2)···O (4 B), with a distance of 2.830 (4) Å, and an angle of 154.9° (with a symmetry transformation used to generate equivalent atoms of -x+1,-y+1,-z+1). In compound 5, the interaction donor and acceptor is between the oxygen atom of the hydroxyethyl group and one oxygen atom of the $(CF_3SO_3)^-$ anion, O (2)···O (5), with a distance of 2.9247 (1) Å and an angle of 167.6° (with a symmetry transformation used to generate equivalent atoms of -x,y+1/2,-z+3/2).

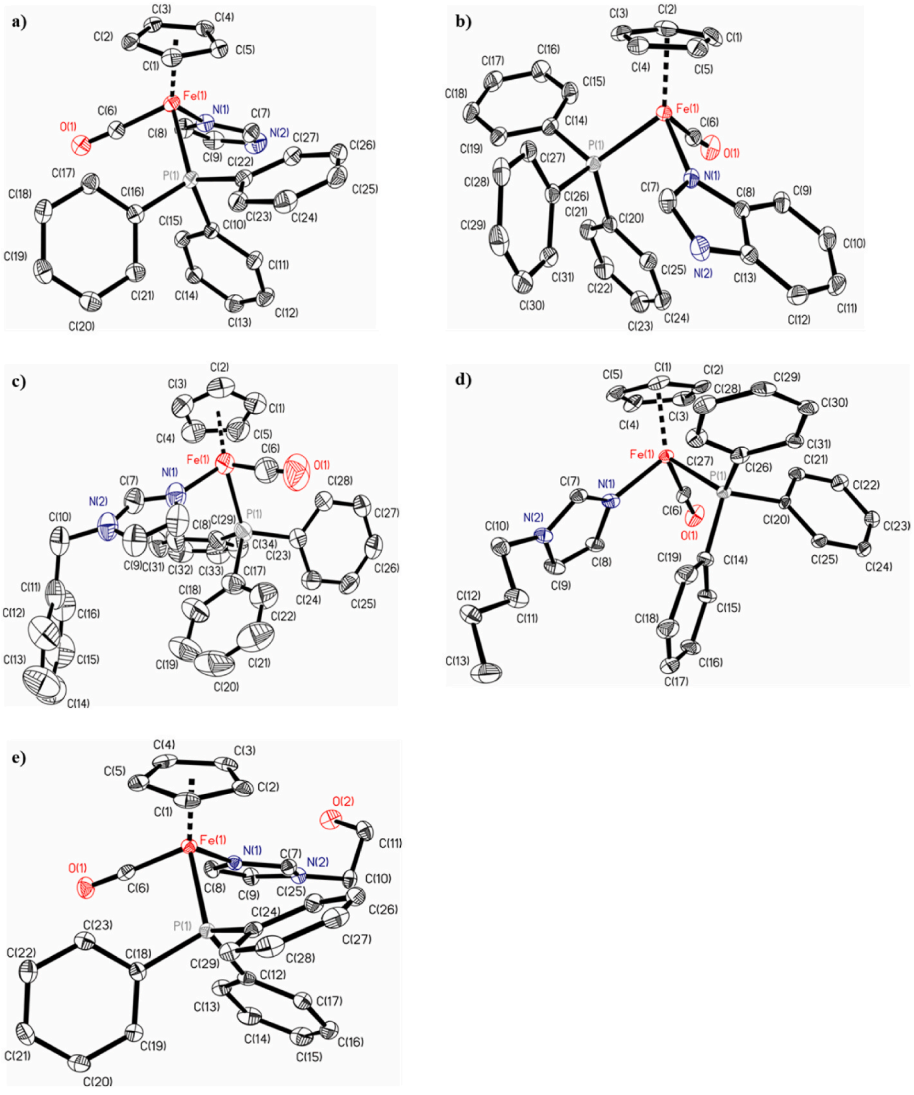

Fig. 2. ORTEP for the cations complexes in the compounds a) [Fe(η^5-C_5H_5) (CO) (PPh_3) (1H-imidazole)](CF_3SO_3) (1); b) [Fe(η^5-C_5H_5) (CO) (PPh_3) (1H-1,3-benzodiazole)](CF_3SO_3) (2); c) [Fe(η^5-C_5H_5) (CO) (PPh_3) (1-benzylimidazole)](CF_3SO_3) (3); d) [Fe(η^5-C_5H_5) (CO) (PPh_3) (1H-1-butylimidazole)](CF_3SO_3) (4); e) [Fe(η^5-C_5H_5) (CO) (PPh_3) (1H-1-(2-hydroxyethyl)imidazole)](CF_3SO_3) (5). All the non-hydrogen atoms are presented by their 50% probability ellipsoids. Hydrogen atoms are omitted for clarity.

2.6. Biological evaluation of the compounds

2.6.1. Stability in solution

All five new compounds have been characterized in terms of their stability towards DMSO, the co-solvent used in biological studies, and in a solution of cell culture medium (DMEM) containing 5% (v/v) DMSO using UV–visible and ^{31}P NMR spectrophotometry. As can be seen in the SI (Figs. S17–S27), under these conditions, the spectral changes were very small during the first hours in both conditions (observed absorbance variations were less than 6%). At 24 h some free PPh_3 could be noticed for some compounds by ^{31}P NMR (spectra in dmso-d6). Overall, the results suggest that all compounds are stable to pursue for biological studies.

2.6.2. Analysis of the cytotoxicity in colon cancer cell lines

The cytotoxic activity of the new [Fe(η^5-C_5H_5)(CO)(PPh_3)(Imi-R)][CF_3SO_3] compounds was assessed in the doxorubicin sensitive (Colo205) and doxorubicin resistant (Colo320) human colon adenocarcinoma cell lines and in the non-cancerous human embryonic lung fibroblasts (MRC5) (Table 2). All cells were incubated for 48 h with different concentrations of the iron compounds. These cancer cell lines were chosen due to their difference in ABCB1 efflux pump expression. Furthermore, the third cell line is a normal cell line to detect the selectivity of the compounds towards cancer cells. The selectivity index (SI) was calculated based on the IC_{50} values of normal and sensitive or resistant cancer cell lines: SI < 1 values denote lack of selectivity, 1 < SI < 3 mean slight selectivity; 3 < SI < 6 values indicate moderate selectivity, whereas values of SI > 6 indicate that compounds are strongly selective (Table 1). All compounds are cytotoxic in both cancer lines showing IC_{50} values in the low micromolar range. The compounds bearing the most lipophilic imidazole-based ligands are those affording the most cytotoxic compounds (3–4), better than cisplatin and in the same order of magnitude than doxorubicin. Even though compound 1 shows a lower IC_{50} (9.63 ± 0.36 μM) in Colo205 cells, it is better in the resistant cell line Colo320, contrarily to the remaining compounds of this family.

Slight selectivity towards both cancer cell lines was observed in case of 1–4, being 3 and 4 the most selective derivatives in this group on the sensitive cell line (SI 21.46 and 2.75, respectively). Only derivative 5 exerted moderate selectivity on the sensitive cancer cell line, however it was not selective towards the resistant cancer cell line.

2.6.3. Inhibition of ABCB1, P-glycoprotein

The effect of the complexes on the ABC-transporter *P*-glycoprotein (ABCB1, *P*-gp) efflux pump was monitored via the rhodamine 123 fluorometric accumulation assay. The third-generation noncompetitive *P*-glycoprotein inhibitor, tariquidar, was used as a positive control [37]. Based on this assay compounds 1–4 could inhibit the activity of ABCB1

Table 1
IC_{50} values determined at 48 h incubation of iron compounds (1–5) against Colo205: doxorubicin sensitive human colon adenocarcinoma cell lines, Colo320: doxorubicin resistant human colon adenocarcinoma cell line and MRC5: human embryonic fibroblast cell lines. Selectivity index: ratio of the IC_{50} values obtained on the non-cancerous and the cancer cells.

Compounds	IC_{50} (μM)			Selectivity Index	
	Colo205	Colo320	MRC5	MRC5/Colo205	MRC5/Colo320
1	9.63 ± 0.36	8.99 ± 0.58	16.68 ± 3.53	1.73	1.86
2	5.23 ± 0.45	5.82 ± 0.82	5.99 ± 0.43	1.15	1.03
3	1.26 ± 0.11	2.21 ± 0.26	3.10 ± 1.09	2.46	1.40
4	1.57 ± 0.05	3.32 ± 0.22	4.30 ± 0.23	2.75	1.30
5	8.01 ± 0.58	26.66 ± 0.91	25.41 ± 4.60	3.17	0.95
cisplatin	5.60 ± 021	3.84 ± 0.20	2.97 ± 0.11	0.53	0.77
doxorubicin	1.2 ± 0.05	1.75 ± 0.36	1.28 ± 0.19	1.07	0.73

Table 2
ABCB1 modulating activity of the compounds in resistant Colo320 cells.

Compounds	Concentration (μM)	FSC	SSC	FL-1	FAR
Tariquidar	0.2	1791	966	121.000	61.111
1	2	1839	921	4.660	2.354
	20	1863	909	21.100	10.657
2	2	1695	803	15.800	7.980
	20	1624	803	21.300	10.758
3	2	1732	834	17.000	8.586
	20	1751	765	31.600	15.960
4	2	1585	740	6.490	3.278
	20	1644	741	19.000	9.596
5	2	1572	755	2.420	1.222
	20	1611	756	4.350	2.197
DMSO	2% (v/v)	1568	751	1.930	0.975

FSC: forward scatter count, SSC: side scatter count, FL-1: fluorescence intensity, FAR: fluorescence activity ratio.

in a dose-dependent manner (Table 2). The highest intracellular accumulation of the ABCB1 substrate rhodamine 123 was detected in the case of compound 3 at 20 μM. Interestingly, very potent ABCB1 inhibition was observed at 2 μM in the presence of compounds 2 and 3, confirmed by the high fluorescence accumulation ratios (FAR) values of 7.98 and 8.586, respectively.

2.6.4. Apoptosis induction

The cell death mechanism of the new iron compounds was assessed using the annexin V/propidium iodide (AV/PI) cytometry-based assay in the resistant Colo 320 cell line at 3 h incubation at 2 and 10 μM. Annexin V is a marker of early apoptosis, while PI is a marker of necrosis. At 2 μM none of the compounds induced apoptosis (Table S4). At 10 μM, two compounds were effective regarding reversal of apoptosis resistance (Table 3). The most potent apoptosis inducer was compound 3 causing early (27.9%) and late apoptosis (34.4%) in the resistant Colo 320 cell line (Fig. 3). Since there is a connection between *P*-glycoprotein (ABCB1) expression and apoptosis resistance [38], it is not surprising that the most effective ABCB1 inhibitor 3 was the most powerful apoptosis inducer. The expression of ABCB1 is related to the apoptosis resistance and the inhibition of this pump can lead to pro-apoptotic activity. Furthermore, compound 4 could induce moderate early apoptosis (7.17%) and this activity can also be explained by the ABCB1 inhibitory effect of this derivative.

2.6.5. Cellular accumulation assay

Compounds 1, 3 and 5 were selected for cellular accumulation assay in Colo205 and Colo320 cells to explore differences between the levels of iron uptake in the case of complexes with different cytotoxic activity (Table 1). The iron concentration was determined by ICP-MS and ICP-OES methods. (Data for other elements obtained by ICP-OES methods are shown in Table S5.) Results are shown in Table 4 for the metal complexes and for the control. The drug-sensitive and the doxorubicin resistant cells displayed a different iron uptake profile for the complexes. The increase of the determined iron concentration was insignificant for complex 3 in the Colo205 cells, and for complexes 1 and 5 in the Colo320 cells in comparison to the control. However, the Colo205 cells showed remarkable iron uptake in the case of complexes 1 and 5 as 7- or 11-fold and 6- or 11-fold higher concentrations were obtained according to both the ICP-MS and ICP-OES data, respectively. Interestingly, the higher iron level does not show relationship with the IC_{50} values, as complexes 1 and 5 were less cytotoxic than complex 3. A slight increase of the iron level (3-fold (ICP-MS) and 4-fold (ICP-OES)) for complex 3 in Colo320 cells was found. In this cell line this complex was the most active among complexes 1, 3 and 5 and the one presenting *P*-gp inhibition. Thus, this result reinforces the previous observations.

3. Conclusions

Multidrug resistance (MDR) is one of the major causes of cancer treatment failure, in particular for aggressive and metastatic cancers. In this frame, we developed a new family of iron(II)-Cp complexes bearing imidazole-based ligands which was fully characterized and studied against cancer cell lines expressing the ABCB1 efflux pump, a key player in cancer MDR. The chosen cell lines were the doxorubicin-sensitive (Colo205) and doxorubicin-resistant (Colo320) human colon

Table 3
Percentage of Colo320 cells in each state after treatment with complexes 1–5 at 10 μM for 3 h. Apoptosis induction in resistant Colo320 cells by annexin-V-FITC and propidium iodide staining. The positive control M627 was used at 20 μM.

Control	% Apoptotic cells AV^+/PI^-	% Late apoptotic cells AV^+/PI^+	% Necrosis AV^-/PI^+
	2.42	2.6	0.622
1	2.56	3.14	0.757
2	3.34	2.65	0.663
3	27.9	34.4	2.25
4	7.17	2.81	0.442
5	2.86	3.55	1.06
M627	7.80	10.0	4.63

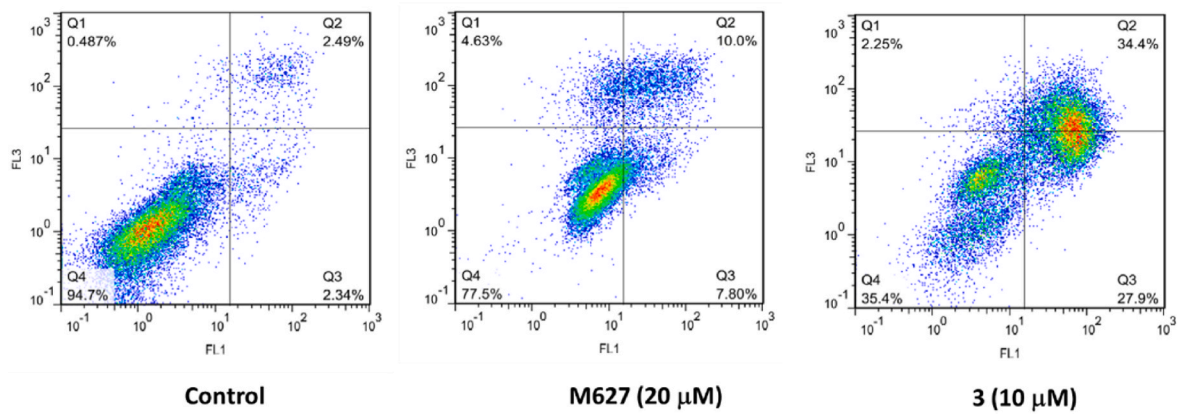

Fig. 3. Apoptosis induction in Colo 320 cells in the presence of 3 at 10 μM. 12H-benzo [α]phenothiazine (M627) was applied as a positive control at 20 μM. Cell populations: necrotic and dead cells are in Q1 (annexin V−/PI+), viable cells are in Q4 (annexin V−/PI−), early apoptotic cells are in Q3 (annexin V+/PI−), and late apoptotic cells are in Q2 (annexin V+/PI+) cells.

Table 4
Cellular iron uptake analysis by ICP-MS and ICP-OES measurements in Colo205 and Colo320 cells.

Compounds	Colo205 (ppm)		Colo320 (ppm)	
	ICP-MS	ICP-OES	ICP-MS	ICP-OES
1	9.35 ± 4.25	9.74 ± 4.10	2.07 ± 0.21	2.27 ± 0.23
3	1.75 ± 0.18	2.09 ± 0.30	4.53 ± 2.33	4.25 ± 1.90
5	7.70 ± 0.20	7.69 ± 0.88	2.01 ± 0.14	2.01 ± 0.16
control	1.33 ± 0.13	1.62 ± 0.16	1.37 ± 0.09	1.53 ± 0.38

adenocarcinoma cells, the latter with ABCB1 expression. Even if all of five half-sandwich Fe(II)-cyclopentadienyl complexes containing imidazole-based ligands showed IC_{50} values in the micromolar range, from all the data gathered, one compound emerged as a leader for this family, namely, [Fe(η^5-C_5H_5)(CO)(PPh_3)(1-benzylimidazole)][CF_3SO_3], 3. Besides showing better IC_{50} than cisplatin and comparable IC_{50} to doxorubicin, it was also slightly selective against the cancer cells (vs. MRC5 human embryonic fibroblast cell lines). Most importantly, it was found to be a very potent ABCB1 inhibitor, induced apoptosis and the iron accumulation within cells was higher in the resistant cell line than in the sensitive one. Structurally, compound 3 bears a lipophilic arm at the imidazole and has the strongest MLCT band, suggesting that this higher electronic delocalization density on the imidazole ring might eventually favor the interactions at the cancer cell targets. Overall, these results suggest that compound 3 is a very promising candidate for future studies aiming at understanding its mechanism of action. As far as we are aware, this is the first iron organometallic compound acting as ABCB1 inhibitor.

4. Materials and methods

All of the organometallic syntheses were carried out under nitrogen atmosphere using standard Schlenk techniques. All solvents used for the organometallic synthesis were freshly distilled under nitrogen atmosphere before use, according to common literature methods, except for dichloromethane and *n*-hexane (used for the synthesis and work-up) that were dried using a MBRAUN solvent purification system (MB SPS-800, M Braun InertgasSysteme GmbH, Garching, Germany). The NMR spectra were obtained on a Brucker Advance 400 spectrometer (^{1}H, 400 M*Hz*; ^{13}C{^{1}*H*}-apt, 100.62 M*Hz*; ^{31}P{^{1}*H*}, 161.97 M*Hz*) at probe temperature (298 K). ^{1}H and ^{13}C chemical shifts were reported downfield from the residual solvent peak, whereas the ^{31}P NMR chemical shifts were reported downfield from the external standard 85% H_3PO_4. All the resonances were characterized for their chemical shifts (δ), given in parts-per-million (ppm), and for their coupling constants (J) expressed in Hertz (*Hz*). Resonance multiplicity is expressed, as follows: singlet (s), doublet (d), triplet (t), multiplet (m), and complex (comp). All the assignments were attributed using HMBC, HMQC, and COSY 2D-NMR techniques. Each sample was prepared under air and at room temperature, while using the most adequate deuterated solvent. The electronic UV–Vis spectra were recorded in dimethylsulfoxide solutions (10^{-3}–10^{-5} M), under air, using 1 cm optical path quartz cells on a Jasco V-660 spectrometer (Elnor, Porto, Portugal) in the range of 200–800 nm. The infrared spectra were recorded in a Shimadzu IRAffinity-1 FTIR spectrophotometer (Kyoto, Japan) in dry KBr pellets, under air, and at room temperature. Elemental analyses were obtained at Laboratório de Análises, Instituto Superior Técnico, using a Fisons Instruments EA1108 system (Fison Instruments Ltd., Glasgow, UK). Data acquisition, integration, and handling were performed using a PC with the software package EAGER-200 (Carlo Erba Instruments).

For the thin layer chromatography (TLC-PET) analytical assays, aluminum oxide on PET of several appropriate dimensions were used. The elution of these plates was performed while using different proportions of acetone/*n*-hexane. Upon elution, the TLC plates were observed under UV light at 254 and 366 nm.

4.1. Synthesis

The synthesis of starting materials [Fe(η^5-C_5H_5)$(CO)_2$I] and [Fe(η^5-C_5H_5)(CO)(PPh_3)I] was done using the commercially available dimer [Fe(η^5-C_5H_5)$(CO)_2]_2$, following the literature procedure [34].

4.1.1. General procedure for the synthesis of [Fe(η^5-C_5H_5)(CO)(PPh_3)(Imi-R)]$^+$, complexes 1-5

To a Schlenk containing a solution of [Fe(η^5-C_5H_5)(CO)(PPh_3)I] (300 mg, 0.56 mmol) in acetone (30 ml) $AgCF_3SO_3$ (215 mg, 0.84 mmol) was added. The solution was stirred for 1 h protected from light. Then this solution was filtered to another Schlenk where the respective imidazole (0.84 mmol) was added (Imi-R = 1*H*-midazole (1); 1*H*-1,3-benzodiazole (2); 1-benzylimidazole (3); 1-butylimidazole (4); 1-(2-hydroxyethyl)imidazole (5)). The reaction mixture was allowed to stir for 1 day at room temperature. The reaction was followed by NMR until all the precursor was found to have been consumed and only a single 'Cp' signal remained. At the end of the reaction, the solution is filtered, and all the solvent is evaporated. The product is redissolved in a mixture of acetone/*n*-hexane (the proportion of these two solvents varied depending on imidazole used), and the product is passed through a neutral alumina column. The orange fraction is collected from the column. The solution is then evaporated, and the red products were recrystallized from acetone/*n*-hexane, and obtained in 44–73% yields.

$[Fe(\eta^5\text{-}C_5H_5)(CO)(PPh_3)(1H\text{-midazole})][CF_3SO_3]$ (1)

For the column chromatography a mixture of acetone/*n*-hexane (3:2) was used. The product was recrystallized from acetone/*n*-hexane, from where crystals for single crystal X-ray diffraction were obtained.

Yield: 45%, Red crystalline powder.

^{1}H NMR [$(CD_3)_2CO$-d_6, Me_4Si, δ/ppm]: 12.07 (s, 1H, H_1); 7.66 (s, 1H, H_2); 7.50 (comp, 6H, Hortho-PPh_3); 7.40 (comp, 3H, Hpara-PPh_3); 7.28 (comp, 6H, Hmeta-PPh_3); 7.12 (comp, 1H, H_5); 7.37 (d, 2, H_3); 6.91 (comp, 1H, H_4); 5.01 (s, 5H, (η^5-C_5H_5)).^{13}C RMN [$(CD_3)_2CO$-d_6, Me_4Si, δ/ppm]: 220.34 (d, $^2J_{CP}$ = 30, C═O); 135.38 (s, C_4); 133.93(d, $^3J_{CP}$ = 10, Cmeta-PPh_3); 133.50 (d,$^1J_{CP}$ = 43, Cipso-PPh_3); 131.90 (d, $^4J_{CP}$ = 3, Cpara-PPh_3); 129.90 (d, $^2J_{CP}$ = 10, Cortho-PPh_3); 120.12 (s, C_5); 85.23 (s, (η^5-C_5H_5)). ^{31}P NMR [$(CD_3)_2CO$-d_6, H_3PO_4, δ/ppm]: 66.308 (s, *P*-PPh_3). FTIR [KBr cm^{-1}]: ν(*N*–H) 3482; ν(*C*–H aromatics) 3142, 2965; ν(C═O) 1962; ν(C═C) 1435; ν($CF_3SO_3^-$) 1252, 1161, 1028; ν(=C–H) 751, 698, 637. UV–Vis in DMSO, λ_{max}/nm [ε/M^{-1}cm^{-1}]: 284 (4625); 345 (790); 415 (720); 536 (250). ESI-MS: (+, *m/z*) Calc for $[C_{27}H_{24}FeN_2OP]^+$: 479.10; Found: 479.10.

$[Fe(\eta^5\text{-}C_5H_5)(CO)(PPh_3)(1H\text{-}1,3\text{-benzodiazole})][CF_3SO_3]$ (2)

For the column chromatography a mixture of acetone/*n*-hexane (2:1) was used. The product was recrystallized from acetone/*n*-hexane, and crystals for single crystal X-ray diffraction were obtained from dichloromethane/*n*-hexane.

Yield: 73%, Red crystalline powder.

^{1}H NMR [$(CD_3)_2CO$-d_6, Me_4Si, δ/ppm]: 12.29 (s, 1H, H_1); 8.20 (d, 1H, $^3J_{HH}$ = 8, H_9); 7.92 (s, 1H, H_2); 7.61 (d, 1H, H_6); 7.58 (comp, 3H, Hpara-PPh_3); 7.50–7.38 (comp, 8H, Hortho-PPh_3+H_7+H_8); 7.26 (comp, 6H, Hmeta-PPh_3); 5.14 (s, 5H, (η^5-C_5H_5)). ^{13}C NMR [$(CD_3)_2CO$-d_6, Me_4Si, δ/ppm]: 221.34 (d, $^2J_{CP}$ = 31, C═O); 144.55 (s, C_4) 134.13 (s, C_5); 133.93 (d,$^3J_{CP}$ = 10, Cmeta-PPh_3); 133.39 (d, $^1J_{CP}$ = 43, Cipso-PPh_3); 132.10 (d,$^4J_{CP}$ = 3, Cpara-PPh_3); 130.06 (d,$^2J_{CP}$ = 10, Cortho-PPh_3); 125.42 (s, C_8); 124.67 (s, C_7); 119.31 (s, C_9); 114.15 (C_6); 85.23 (s, (η^5-C_5H_5)). ^{31}P NMR [$(CD_3)_2CO$-d_6, H_3PO_4, δ/ppm]: 65.37 (s, *P*-PPh_3). FTIR [KBr cm^{-1}]: ν(*N*–H) 3490; ν(*C*–H aromatics) 3115, 3068, 2966, 2941; 2860 ν(C═O) 1961; ν(C═C) 1458, 1409; ν($CF_3SO_3^-$) 1246, 1160, 1028; ν(=C–H) 705, 638. UV–Vis in DMSO, λ_{max}/nm [ε/M^{-1}cm^{-1}]: 285 (5950); 349 (Sh); 415(945); 539 (316). Elemental analysis (%) Calc. $C_{32}H_{26}F_3FeN_2O_4PS$ (678,44): C: 56.6; H: 3.9; N: 4.1; S: 4.7. Found: C: 56.2; H: 3.9; N: 4.2; S: 5.0.

$[Fe(\eta^5\text{-}C_5H_5)(CO)(PPh_3)(1\text{-benzylimidazole})][CF_3SO_3]$ (3)

For the column chromatography a mixture of acetone/*n*-hexane (3:1) was used. The product was recrystallized from acetone/*n*-hexane, from where crystals for single crystal X-ray diffraction were obtained.

Yield: 55%, Red crystalline powder.

^{1}H NMR [$(CD_3)_2CO$-d_6, Me_4Si, δ/ppm]: 7.91 (s, 1H, H_2); 7.56 (comp, 3H, Hpara-PPh_3); 7.46 (comp, 6H, Hortho-PPh_3); 7.36 (comp, 3H, *H10*+*H9*); 7.25 (comp, 6H, *H*meta-PPh_3); 7.17 (comp, 2H, *H8*); 7.13 (s, 1H, H_5); 6.88 (s, 1H, H_4); 5.14 (s, 2H, C_6); 5.00 (s, 5H, (η^5-C_5H_5)). ^{13}C NMR [$(CD_3)_2CO$-d_6, Me_4Si, δ/ppm]: 220.24 (d,$^2J_{CP}$ = 30, C═O); 136.91 (s, C_7); 136.37 (s, C_4) 133.93 (d,$^3J_{CP}$ = 10, Cmeta-PPh_3); 133.41 (d,$^1J_{CP}$ = 44, Cipso-PPh_3); 131.92 (d,$^4J_{CP}$ = 3, Cpara-PPh_3); 129.89 (d,$^2J_{CP}$ = 10, *C*ortho-PPh_3); 129.80 (s, C_{10}); 129.23 (s, C_9); 123.12 (s, C_5); 85.27 (s, (η^5-C_5H_5)); 52.07 (s, C_6). ^{31}P NMR [$(CD_3)_2CO$-d_6, H_3PO_4, δ/ppm]: 66.24 (s, *P*-PPh_3). FTIR [KBr cm^{-1}]: ν(*N*–H) 3480; ν(*C*–H aromatics) 3116, 3101, 3055; ν(C═O) 1961; ν($CF_3SO_3^-$) 1263, 1163, 1031; ν(=C–H) 705, 638. UV–Vis in DMSO, λ_{max}/nm [ε/M^{-1}cm^{-1}]: 278 (*Sh*); 290 (Sh); 332 (968); 416 (935); 535 (332). Elemental analysis (%) Calc. For $C_{35}H_{30}F_3FeN_2O_4PS$ (718.51): C: 58.5; H: 4.2; N: 3.9; S: 4.4. Found: C: 58.0; H: 4.2; N: 4.0; S: 4.0.

$[Fe(\eta^5\text{-}C_5H_5)\ (CO)\ (PPh_3)\ (1\text{-butylimidazol})][CF_3SO_3]$ (4)

For the column chromatography a mixture of acetone/*n*-hexane (2:1) was used. The product was recrystallized from acetone/*n*-hexane, and crystals for single crystal X-ray diffraction were obtained from dichloromethane/*n*-hexane.

Yield: 44%, Red crystalline powder.

^{1}H NMR [$(CD_3)_2CO$-d_6, Me_4Si, δ/ppm]: 7.71 (s, 1H, H_2); 7.59 (comp, 3H, Hpara-PPh_3); 7.52 (comp, 6H, Hortho-PPh_3); 7.28 (comp, 6H, Hmeta-PPh_3); 7.13 (s, 1H, H_4); 6.91 (s, 1H, H_5); 5.00 (d, $^3J_{HH}$ = 2, 5H, (η^5-C_5H_5)); 3.91 (t,$^3J_{HH}$ = 7.26, 2H, H_6), 1.56 (m, 2H, H_7); 1.13 (m, 2H, H_8); 0.86 (t, $^3J_{HH}$ = 7.39, 3H, H_9). ^{13}C NMR [$(CD_3)_2CO$-d_6, Me_4Si, δ/ppm]: 220.28 (d,$^2J_{CP}$ = 30, C═O); 136.08 (s, C_4) 133.99 (d,$^3J_{CP}$ = 10, Cmeta-PPh_3); 133.41 (d,$^1J_{CP}$ = 44, Cipso-PPh_3); 131.95 (d,$^4J_{CP}$ = 2, Cpara-PPh_3); 129.93 (d,$^2J_{CP}$ = 10, Cortho-PPh_3); 123.03 (s, C_5); 85.27 (s, (η^5-C_5H_5)); 48.46 (s, C_9); 33.35 (s, C_{10}); 20.07 (s, C_{11}); 13.72 (s, C_{12}). ^{31}P NMR [$(CD_3)_2CO$-d_6, H_3PO_4, δ/ppm]: 66.12 (s, *P*-PPh_3). FTIR [KBr cm^{-1}]: ν(*N*–H) 3480; ν(*C*–H aromatics) 3126, 3084, 3059, 2954, 2930, 2873; ν(C═O) 1955; ν(C═C) 1458, 1409; ν($CF_3SO_3^-$) 1263, 1224, 1155, 1031; ν(=C–H) 696, 638. UV–Vis in DMSO, λ_{max}/nm [ε/M^{-1}cm^{-1}]: 271 (9532); 345 (Sh); 413 (732); 538 (240). Elemental analysis (%) Calc. For $C_{32}H_{32}F_3FeN_2O_4PS$ (684.49): C: 56.1; H: 4.7; N: 4.1; S: 4.6. Found: C: 55.8; H: 4.8; N: 4.0; S: 4.0.

$[Fe(\eta^5\text{-}C_5H_5)(CO)(PPh_3)(1\text{-}(2\text{-hidroxyethyl})\text{imidazole})][CF_3SO_3]$ (5)

For the column chromatography a mixture of acetone/*n*-hexane (2:1), was used. An increasing proportion of acetone is used until the product is completely extracted. The product was recrystallized from acetone/*n*-hexane, and crystals for single crystal X-ray diffraction were obtained from dichloromethane/*n*-hexane.

Yield: 63%, Red crystalline powder.

^{1}H NMR [$(CD_3)_2CO$-d_6, Me_4Si, δ/ppm]: 7.70 (s, 1H, H_2); 7.57 (comp, 3H, Hpara-PPh_3); 7.51 (comp, 6H, Hortho-PPh_3); 7.29 (comp, 6H, Hmeta-PPh_3); 7.10 (s, 1H, H_5); 6.81 (s, 1H, H_4); 5.00 (d,$^3J_{HH}$ = 2, 5H, (η^5-C_5H_5)); 4.15 (t, $^3J_{HH}$ = 5, 1H, –OH); 4.00 (d, $^3J_{HH}$ = 18, 2H, H_6); 3.67 (q,$^3J_{HH}$ = 18, 2H, H_6). ^{13}C NMR [$(CD_3)_2CO$-d_6, Me_4Si, δ/ppm]: 220.29 (d,$^2J_{CP}$ = 30, C═O); 135.63 (s, C_4) 134.00 (d,$^3J_{CP}$ = 10, Cmeta-PPh_3); 133.50 (d,$^1J_{CP}$ = 44, Cipso-PPh_3); 131.88 (d,$^4J_{CP}$ = 3, Cpara-PPh_3); 129.80 (d,$^2J_{CP}$ = 10, Cortho-PPh_3); 123.45 (s, C_5); 85.22 (s, (η^5-C_5H_5)); 61.60 (s, C_7); 51.27 (s, C_6). ^{31}P NMR [$(CD_3)_2CO$-d_6, H_3PO_4, δ/ppm]: 66.24 (s, *P*-PPh_3). FTIR [KBr cm^{-1}]: ν(*O*–H) 3500; ν(*N*–H) 3464; ν(*C*–H aromatics) 3122, 3101, 2922, 2930, 2872; ν(C═O) 1959; ν(C═C) 1525, 1286; ν($CF_3SO_3^-$) 1255, 1224, 1155, 1029; ν(=C–H) 698, 634. UV–Vis in DMSO, λ_{max}/nm [ε/M^{-1}cm^{-1}]: 280 (5786); 340 (Sh); 416 (884); 538 (325). Elemental analysis (%) Calc. For $C_{30}H_{28}F_3FeN_2O_5PS$ (672.43): C: 53.6; H: 4.2; N: 4.2; S: 4.8. Found: C: 53.5; H: 4.1; N: 4.1; S: 5.0.

4.2. X-ray crystal structure determination

Three-dimensional X-ray data were collected on a Bruker Kappa Apex CCD diffractometer at low temperature for compounds 1, 2, 4 and 5 and at 250 K for compound 3 by the φ-ω scan method. Reflections were measured from a hemisphere of data collected from frames, each of them covering 0.3° in ω. A total of 52,658 for 1, 84,144 for 2, 45,409 for 3, 15,926 for 4 and 26,644 for 5 reflections measured were corrected for Lorentz and polarization effects and for absorption by multi-scan methods based on symmetry-equivalent and repeated reflections. Of the total, 5527 for 1, 6292 for 2, 5773 for 3, 12,848 for 4 and 4903 for 5 independent reflections exceeded the significance level ($|F|/\sigma|F|$) > 4.0. After data collection, a multi-scan absorption correction (SADABS) [39] was applied in each case. The structures of the compounds were solved by direct methods and refined by full matrix least-squares on F^2 data using Olex2 [40,41]. SHELX suite of programs were used for drawing the structures [42]. Hydrogen atoms were included in calculation position and refined in the riding mode. Refinements were done with allowance for thermal anisotropy of all non-hydrogen atoms. Compounds 2, 3 and 4 present a disorder, on $(CF_3SO_3)^-$ anion in compound 2 and 3, and on butyl group in compound 4. These disorders were refined, and two atomic sites were observed and refined for the atoms implied with the

anisotropic atomic displacement parameters. More specifically these disorders were refined using 153, 55, and 72 restraints, respectively (SADI, SIMU and DELU restraints were used). The site occupancy factors were 0.748636 for S (1 A)-O (2 A)-O (3 A)-O (4 A)-F (1 A)-F (2 A)-F (3 A) in compound 2, 0.56615 for O (3 A) and 0.20139 for F (2 A)-F (3 A) in compound 3 and 0.52247 for C (41 A)-C (42 A)-C (43 A) in compound 4. A final difference Fourier map showed no residual electronic density: 0.63 and −0.50 e. Å^{-3} for 2, 0.76 and −0.54 e. Å^{-3} for 3 and 0.42 and −0.45 for 5. In compounds 1 and 4, the final difference Fourier map showed a residual electronic density: 1.32 and −0.67 e. Å^{-3} for 1 and 1.35 and −1.13 e. Å^{-3} for 4, next to the metal atoms in both cases. Weighting schemes of $w = 1/[\sigma\ [2](F_o^2) + (0.035699\ P)\ [2] + 4.970706\ P]$ for 1, $1/[\sigma\ [2](F_o^2) + (0.02869\ P)\ [2] + 0.987544\ P]$ for 2, $1/[\sigma\ [2](F_o^2) + (0.040081\ P)\ [2] + 8.238848\ P]$ for 3, $1/[\sigma\ [2](F_o^2) + (0.181354\ P)\ [2] + 3.27114\ P]$ for 4 and $1/[\sigma\ [2](F_o^2) + (0.024305\ P)\ [2] + 1.751071\ P]$ for 5, where $P = (|F_o|\ [2] + 2|F_c|\ [2])/3$, were used in the latter stages of refinement. Further details of the crystal structure determination are given in Table 1. CCDC 2248313–2248,317 contain the supplementary crystallographic data for the structures reported in this paper. These data can be obtained free of charge via http://www.ccdc.cam.ac.uk/conts/retrieving.html, or from the Cambridge Crystallographic Data Center, 12 Union Road, Cambridge CB2 1EZ, UK; fax: (+44) 1223 336 033; or e-mail: deposit@ccdc.cam.ac.uk. Supplementary data associated with this article can be found, in the online version, at doi: 10.1016/j.ejmech.2023.115466.

4.3. Biological studies

4.3.1. Cell cultures

The human colon adenocarcinoma cell lines, the Colo205 (ATCC-CCL-222) doxorubicin-sensitive and Colo 320/MDR-LRP (ATCC-CCL-220.1) resistant to doxorubicin expressing ABCB1, were purchased from LGC Promochem (Teddington, UK). The cells were cultured in RPMI-1640 medium supplemented with 10% heat-inactivated fetal bovine serum (FBS), 2 mM L-glutamine, 1 mM Na-pyruvate, 10 mM Hepes, nystatin and a penicillin-streptomycin mixture. The MRC-5 (ATCC CCL-171) human embryonic lung fibroblast cell line (LGC Promochem) was cultured in EMEM medium, supplemented with 1% non-essential amino acid (NEAA) mixture, 10% heat-inactivated FBS, 2 mM L-glutamine, 1 mM Na-pyruvate, nystatin, and a penicillin-streptomycin mixture. The cell lines were incubated in a humidified atmosphere (5% CO_2, 95% air) at 37 °C.

4.3.2. Compounds dilution and storage

Compounds 1–5 were dissolved in DMSO as 10 mM solutions. Aliquots were prepared and stored at −20 °C and protected from light.

4.3.3. Assay for cytotoxic effect

Prior to the assay the cells were seeded overnight in 96-well flat-bottomed microtiter plates: 6 × 10^3 of human colonic adenocarcinoma cells in 100 μL of the medium (RPMI-1640) and adherent human embryonic lung fibroblast cell line (6 × 10^3/well) in EMEM. The effects of increasing concentrations of the compounds on cell growth were tested in 96-well flat-bottomed microtiter plates. The two-fold serial dilutions of the tested compounds were made starting with 100 μM. The serial dilutions of the compounds were made in a separate plate starting with 100 μM, and then transferred to the plates containing the adherent corresponding cell line. Culture plates were incubated at 37 °C for 48 h; at the end of the incubation period, 20 μL of MTT (thiazolyl blue tetrazolium bromide) solution (from a 5 mg/ml stock solution) were added to each well. After incubation at 37 °C for 4 h, 100 μL of sodium dodecyl sulfate (SDS) solution (10% SDS in 0.01 M HCl) were added to each well and the plates were further incubated at 37 °C overnight. Cell growth was determined by measuring the optical density (OD) at 540 nm (ref. 630 nm) with Multiscan EX ELISA reader (Thermo Labsystems, Cheshire, WA, USA). Inhibition of cell growth was expressed as IC_{50} values, defined as the inhibitory dose that reduces the growth of the cells exposed to the tested compounds by 50%. IC_{50} values and the SD of triplicate experiments were calculated by using GraphPad Prism software version 5.00 for Windows with nonlinear regression curve fit (GraphPad Software, San Diego, CA, USA; www.graphpad.com).

4.3.4. Rhodamine 123 accumulation assay

The cell numbers of the human colon adenocarcinoma cell lines were adjusted to 2 × 10^6 cells/mL, re-suspended in serum-free RPMI 1640 medium and distributed in 0.5 ml aliquots into Eppendorf centrifuge tubes. The tested compounds were added at 2 or 20 μM concentrations, and the samples were incubated for 10 min at room temperature. Tariquidar was applied as positive control at 0.2 μM. DMSO at 2% v/v was used as solvent control. Next, 10 μL (5.2 μM final concentration) of the fluorochrome and ABCB1 substrate rhodamine 123 (Sigma) were added to the samples and the cells were incubated for a further 20 min at 37 °C, washed twice and re-suspended in 1 ml PBS (phosphate buffered saline) for analysis. The fluorescence of the cell population was measured with a PartecCyFlow® flow cytometer (Partec, Münster, Germany). The fluorescence activity ratio was calculated as the quotient between FL-1 of treated/untreated resistant Colo320 cell line over treated/untreated sensitive Colo205 cell line according to the following equation:

$$FAR = \frac{Colo320_{treated}\ /\ Colo320_{control}}{Colo205_{treated}\ /\ Colo205_{control}}$$

4.3.5. Apoptosis induction

The assay was carried out using Annexin V-fluorescein isothiocyanate (FITC) Apoptosis Detection Kit (Sigma, Merck KGaA, Darmstadt, Germany) according to the manufacturer's instructions. The density of the resistant Colo320 cell suspension was adjusted to approximately 1 × 10^6 cells/ml. The cell suspension was distributed into 0.5 ml aliquots (5 × 10^5 cells) to a 24-well microplate and the compounds were added at a final concentration of 2 and 10 μM. The apoptosis inducer 12*H*-benzo[α]phenothiazine (M627) was applied as a positive control at a final concentration of 20 μM [43]. The cells were incubated in the presence of the compounds for 3 h at 37 °C. The culture medium was removed, the cells were washed with phosphate-buffered saline and fresh medium was added to the cells. The 24-well plates were incubated overnight at 37 °C with 5% CO_2. On the following day, the apoptosis assay was carried out according to the kit protocol by which cells were stained with FITC-labelled annexin V and propidium iodide (PI) and then analyzed by flow cytometry. This discriminated between necrotic (annexin V−/PI+), viable (annexin V−/PI−), early apoptotic (annexin V+/PI−), and late apoptotic (annexin V+/PI+) cells. The fluorescence of cell populations was analyzed immediately using a PartecCyFlow® flow cytometer.

4.3.6. Cellular uptake measurements

For accumulation studies, Colo 205 and Colo320 adenocarcinoma cells were cultured in T25 flasks (10^6 cells/each) in RPMI 1640 medium. The cells were trypsinized, harvested and distributed into 24-well plates (10^6 cells/well), seeded and incubated overnight at 37 °C in a CO_2 incubator. On the following day, the medium was removed, and fresh medium was added to the samples containing the metal complexes at 5 μM. All samples were duplicated under each condition. After 24 h incubation time, the samples were taken out from the incubator, detached with 0.25% of Trypsin-Versen solution. After trypsinization and cell harvesting, the samples were resuspended in RPMI, transferred into Eppendorf tubes and centrifuged. The supernatant was removed, and the cells were kept at −20 °C until the cellular uptake measurements in Eppendorf tubes. For sample preparation, they were transferred into 25 ml beakers and 2 ml of ultrapure 67% HNO_3 (VWR) was added to them. After this, the tubes were washed with 2 × 1 ml of ultrapure water (Suez, 18.2 MΩ/cm), which was then combined with the respective samples. The samples were digested on a hot plate, then filled up to 10 ml with

ultrapure water. Two blanks were prepared alongside the samples. The tubes were weighed before opening, and again after emptying and drying them in an oven, and the sample weights were taken from the weight difference of the two measurements. The elemental analyses were done by two inductively coupled plasma (ICP) methods. Firstly, the samples were measured on a Thermo Fisher ICAP-Q ICP mass spectrometer (MS), equipped with a quadrupole mass analyser and an ASX-520 autosampler unit. Three isotopes of iron (^{54}Fe, ^{56}Fe and ^{57}Fe) were used for quantitative analysis. Four calibration points (0, 1, 10 and 100 μg/L) were prepared for the quantification, the first being ultrapure (18.2 MΩ/cm) water, the others were diluted from a Fe single-element standard solution (CPA-Chem, 1000 mg/L in 2% nitric acid), each point containing 1 ml of ultrapure 67% HNO_3 in a total volume of 50 ml. The final results were obtained after blank subtraction and averaging the measurements at the three isotopes. In addition to the ICP-MS analysis, control measurements of Fe, as well as simultaneous measurement of other elements above quantitation limit (LOQ) was accomplished on a Spectro Genesis simultaneous ICP optical emission spectrometer (OES) with axial plasma viewing and using multielement standard solution (CPA-Chem, 33 elements) for calibration and quantification.

Declaration of competing interest

The authors declare that they have no known competing financial interests or personal relationships that could have appeared to influence the work reported in this paper.

Data availability

Data will be made available on request.

Acknowledgments

This work was funded by *Fundação para a Ciência e a Tecnologia* (FCT), I.P./MCTES through national funds (PIDDAC) - UIDB/00100/2020 and LA/P/0056/2020. This work was also funded in the scope of the project PTDC/QUI-QIN/28662/2017 (FCT). Andreia Valente acknowledges CEECIND 2017 (CEECIND/01974/2017; acknowledging FCT, as well as POPH and FSE—European Social Fund). A. P. thanks FCT for his Ph.D. Grant (SFRH/BD/139412/2018 and COVID/BD/153267/2023). B.R. was supported by the Szeged Foundation for Cancer Research (Szegedi Rákkutatásért Alapítvány). G.S. was supported by the János Bolyai Research Scholarship (BO/00158/22/5) of the Hungarian Academy of Sciences and by the ÚNKP-22-5-SZTE-588 New National Excellence Program of the Ministry for Culture and Innovation from the source of the National Research, Development and Innovation Fund.

Appendix A. Supplementary data

Supplementary data to this article can be found online at https://doi.org/10.1016/j.ejmech.2023.115466.

References

[1] M.M. Heravi, V. Zadsirjan, RSC Adv. 10 (2020) 44247–44311.
[2] G. Li Petri, M.V. Raimondi, V. Spanò, R. Holl, P. Barraja, A. Montalbano, Pyrrolidine in Drug Discovery: A Versatile Scaffold for Novel Biologically Active Compounds, vol. 379, Springer International Publishing, 2021.
[3] N. Kerru, L. Gummidi, S. Maddila, K.K. Gangu, S.B. Jonnalagadda, Molecules 25 (42) (2020) 1909.
[4] I. Ali, M.N. Lone, H.Y. Aboul-Enein, Medchemcomm 8 (2017) 1742–1773.
[5] P. Sharma, C. Larosa, J. Antwi, R. Govindarajan, K.A. Werbovetz, Molecules 26 (66) (2021) 4213.
[6] S.S. Alghamdi, R.S. Suliman, K. Almutairi, K. Kahtani, D. Aljatli, Drug Des. Dev. Ther. 15 (2021) 3289–3312.
[7] E. Alessio, L. Messori, Met. Ions Life Sci. 18 (2018) 141–170.
[8] E. Alessio, Eur. J. Inorg. Chem. 2017 (2017) 1549–1560.
[9] E. Alessio, L. Messori, Molecules 24 (2019) 1–20.
[10] R. Trondl, P. Heffeter, C.R. Kowol, M.A. Jakupec, W. Berger, B.K. Keppler, Chem. Sci. 5 (2014) 2925–2932.
[11] A.S. Basaleh, F.Y. Alomari, A.A. Sharfalddin, N.S. Al-Radadi, D. Domyati, M. A. Hussien, Molecules 27 (21) (2022) 2796.
[12] A.K. Pradhan, A. Shyam, P. Mondal, New J. Chem. 45 (2021) 5682–5694.
[13] P.C. Kunz, M.U. Kassack, A. Hamacher, B. Spingler, Dalton Trans. (2009) 7741–7747.
[14] A. Lewis, M. McDonald, S. Scharbach, S. Hamaway, M. Plooster, K. Peters, K. M. Fox, L. Cassimeris, J.M. Tanski, L.A. Tyler, J. Inorg. Biochem. 157 (2016) 52–61.
[15] A.R.E. Mahdy, O.A. Abu Ali, W.M. Serag, E. Fayad, R.F.M. Elshaarawy, E.M. Gad, J. Mol. Struct. 1259 (2022), 132726.
[16] L. Conti, E. Macedi, C. Giorgi, B. Valtancoli, V. Fusi, Coord. Chem. Rev. 469 (2022), 214656.
[17] S.H. Rasanani, M.E. Moghadam, E. Soleimani, A. Divsalar, D. Ajloo, A. Tarlani, M. Amiri, J. Biomol. Struct. Dyn. 36 (2018) 3058–3076.
[18] N. Ferri, G. Facchetti, S. Pellegrino, C. Ricci, G. Curigliano, E. Pini, I. Rimoldi, Bioorg. Med. Chem. 23 (2015) 2538–2547.
[19] F. Gümüş, Ö. Algül, G. Eren, H. Eroğlu, N. Diril, S. Gür, A. Özkul, Eur. J. Med. Chem. 38 (2003) 473–480.
[20] J. Vančo, Z. Šindelář, Z. Dvořák, Z. Trávníček, J. Inorg. Biochem. 142 (2015) 92–100.
[21] R. Herchel, Z. Indelá, Z. Trávníek, R. Zboil, J. Vančo, Dalton Trans. (2009) 9870–9880.
[22] A.C. Gonçalves, T.S. Morais, M.P. Robalo, F. Marques, F. Avecilla, C.P. Matos, I. Santos, A.I. Tomaz, M.H. Garcia, J. Inorg. Biochem. 129 (2013) 1–8.
[23] A. Valente, T.S. Morais, R.G. Teixeira, C.P. Matos, A.I. Tomaz, M. Helena Garcia, Synthetic Inorganic Chemistry: New Perspectives, 2021, pp. 223–276.
[24] G. Agonigi, L. Biancalana, M.G. Lupo, M. Montopoli, N. Ferri, S. Zacchini, F. Binacchi, T. Biver, B. Campanella, G. Pampaloni, V. Zanotti, F. Marchetti, Organometallics 39 (2020) 645–657.
[25] O.A. Lenis-Rojas, S. Cordeiro, M. Horta-Meireles, J.A.A. Fernández, S.F. Vila, J. A. Rubiolo, P. Cabezas-Sainz, L. Sanchez, A.R. Fernandes, B. Royo, Molecules 26 (2021) 1–14.
[26] D. Rocco, N. Busto, C. Pérez-Arnaiz, L. Biancalana, S. Zacchini, G. Pampaloni, B. Garcia, F. Marchetti, Appl. Organomet. Chem. 34 (2020) 1–18.
[27] S. Braccini, G. Provinciali, L. Biancalana, G. Pampaloni, F. Chiellini, F. Marchetti, Appl. Sci. 11 (10) (2021) 4351.
[28] S. Schoch, S. Braccini, L. Biancalana, A. Pratesi, T. Funaioli, S. Zacchini, G. Pampaloni, F. Chiellini, F. Marchetti, Inorg. Chem. Front. 9 (2022) 5118–5139.
[29] P.R. Florindo, D.M. Pereira, P.M. Borralho, C.M.P. Rodrigues, M.F.M. Piedade, A. C. Fernandes, J. Med. Chem. 58 (2015) 4339–4347.
[30] H.T. Poh, P.C. Ho, W.Y. Fan, RSC Adv. 6 (2016) 18814–18823.
[31] A. Benamrane, B. Herry, V. Vieru, S. Chakraborty, S. Biswas, S. Prince, C. Marschner, B. Blom, J. Organomet. Chem. 934 (2021), 121659.
[32] A.L. Noffke, A. Habtemariam, A.M. Pizarro, P.J. Sadler, Chem. Commun. 48 (2012) 5219–5246.
[33] A. Valente, A.M. Santos, L. Côrte-Real, M.P. Robalo, V. Moreno, M. Font-Bardia, T. Calvet, J. Lorenzo, M.H. Garcia, J. Organomet. Chem. 756 (2014) 52–60.
[34] A. Pilon, P. Gírio, G. Nogueira, F. Avecilla, H. Adams, J. Lorenzo, M.H. Garcia, A. Valente, J. Organomet. Chem. 852 (2017) 34–42.
[35] A. Pilon, A.R. Brás, L. Côrte-Real, F. Avecilla, P.J. Costa, A. Preto, M. Helena Garcia, A. Valente, Molecules 25 (22) (2020) 1592.
[36] A. Pilon, P. Gírio, G. Nogueira, F. Avecilla, H. Adams, J. Lorenzo, M.H. Garcia, A. Valente, J. Organomet. Chem. 852 (2017) 34–42.
[37] P. Kannan, S. Telu, S. Shukla, S.V. Ambudkar, V.W. Pike, C. Halldin, M. M. Gottesman, R.B. Innis, M.D. Hall, ACS Chem. Neurosci. 2 (2011) 82–89.
[38] L.J. Robinson, W.K. Roberts, T.T. Ling, D. Lamming, S.S. Sternberg, P.D. Roepe, Biochemistry 36 (1997) 11169–11178.
[39] G.M. Sheldrick, SADABS, Version 2.10, University of Göttingen, Ger, 2004.
[40] L.J. Bourhis, O.V. Dolomanov, R.J. Gildea, J.A.K. Howard, H. Puschmann, Acta Crystallogr. Sect. A Found. Crystallogr. 71 (2015) 59–75.
[41] O.V. Dolomanov, L.J. Bourhis, R.J. Gildea, J.A.K. Howard, H. Puschmann, J. Appl. Crystallogr. 42 (2009) 339–341.
[42] G.M. Sheldrick, Acta Crystallogr. Sect. C Struct. Chem. 71 (2015) 3–8.
[43] M. Gajdács, G. Spengler, C. Sanmartín, M.A. Marć, J. Handzlik, E. Domínguez-Álvarez, Bioorg. Med. Chem. Lett 27 (2017) 797–802.